RSC Advances

PAPER

View Article Online
View Journal | View Issue

Cite this: *RSC Adv.*, 2017, **7**, 30303

Synthesis of highly substituted dihydro-2-oxopyrroles using Fe_3O_4@nano-cellulose–OPO_3H as a novel bio-based magnetic nanocatalyst†

Naeimeh Salehi and Bi Bi Fatameh Mirjalili *

Received 11th April 2017
Accepted 5th June 2017

DOI: 10.1039/c7ra04101b

rsc.li/rsc-advances

A bio-based magnetic nanocatalyst (Fe_3O_4@nano-cellulose–OPO_3H) has been made *via* immobilization of $-OPO_3H$ groups on a Fe_3O_4@nano-cellulose surface. Fe_3O_4@nano-cellulose was synthesized by co-precipitation of Fe^{3+} and Fe^{2+} salts in an aqueous suspension of nano-cellulose. The catalyst was characterized by FT-IR, FESEM, XRD, TGA, VSM, EDX, XRF and BET. It has been proved that such a heterogeneous catalyst shows high efficiency for the synthesis of dihydro-2-oxopyrrole derivatives *via* four-component reactions of amines, dialkyl acetylenedicarboxylates and aldehydes under mild reaction conditions. The present procedure is a green and environmental friendly approach that offers many advantages including high yield, easy work-up, simple recovery and reusability of the catalyst.

Introduction

The implementation of chemical reactions through greener pathways is one of the main challenges in today's organic chemistry. In this regard, chemists are focusing on the development of new synthetic methodologies using bio-based solvents such as water or ethanol and eco-friendly heterogeneous catalysts.[1–3] On the other hand, multicomponent reactions (MCRs) as a powerful tool play an important role in the development of molecular designs. Such processes promote combinatorial chemistry by forming several bonds in a single operation without the need for time-consuming and expensive purification procedures.[4–7] Due to such benefits, utilizing multicomponent routes is an alternative strategy to develop a simple and green synthesis of organic compounds.

2-Oxodihydropyrroles as an important class of heterocycle compounds have wide biological activities such as antitumor and anticancer,[8] antibiotic,[9] anti-HIV,[10] DNA polymerase inhibition,[11] herbicidal[12] and inhibition of human cytomegalovirus protease.[13] Also, its derivatives are found in the structural cores of many natural bioactive products like bilirubins,[14] pyrrocidine A,[15] oteromycin,[16] talaroconvolutin A,[17] ypaoamide,[18] thiomarinol A4,[19] (Z) pulchellalactam,[20] PI-091 (ref. 21) and Jatropham.[22] Recently, a few protocols to synthesise polyfunctionalized dihydro-2-oxopyrroles *via* the four-component reaction of dialkylacetylenedicarboxylate, aldehyde, and amines have been developed. TiO_2 nanopowder,[23] I_2,[24] AcOH,[25] $Cu(OAc)_2 \cdot H_2O$,[26] [*n*-Bu_4N][HSO_4],[27] trityl chloride (Ph_3CCl),[28] nano-$TiCl_4/SiO_2$,[29] BF_3/nano-sawdust,[30] UiO-66-SO_3H,[31] $CoFe_2O_4$@SiO_2@IRMOF[32] and 2,6-pyridinedicarboxylic acid[33] are applied for synthesis of dihydro-2-oxopyrroles as catalysts. Despite the remarkable achievements, some of these catalysts have many imperfections such as lack of catalyst recyclability, production of large amounts of toxic chemical waste and difficulties in catalyst recovery. Hence, there is a need to prepare an easily recyclable catalyst for the synthesis of dihydro-2-oxopyrroles.

Economically importance and environmentally benign features of magnetic nanoparticles (MNPs) have put them under chemical spotlight. They have several important advantages such as easy preparation and functionalization, high catalytic activity, simple separation using an external magnet and a high degree of chemical stability.[34–36] Among the various magnetic nanoparticles, Fe_3O_4 nanoparticles have been more extensively studied as the core magnetic support due to their stronger magnetic properties, chemical stability, readily available, effortless preparation *via* co-precipitation and low toxicity.[37] It should be noted that pure Fe_3O_4 NPs, with the high surface area to volume ratio, are highly chemically active and suffer from an inherent instability. They are very sensitive to oxidation and tend to aggregate spontaneously when exposed to acids and aqueous solutions. To overcome the above inherent limitations, the surface of nanoparticles can be coated by a suitable protective coating such as polymers, silica or carbon.[38] Cellulose, as a renewable and naturally abundant biopolymer, is one of the most ideal coating layers for Fe_3O_4 NPs because it not only stabilizes the nanoparticles in solution but also enjoys free OH groups for functionalization purposes.[39,40]

Department of Chemistry, Faculty of Sciences, Yazd University, P.O. Box 89195-741, Yazd, Islamic Republic of Iran. E-mail: fmirjalili@yazd.ac.ir; Fax: +98 38210644; Tel: +98 3531232672

† Electronic supplementary information (ESI) available. See DOI: 10.1039/c7ra04101b

In this study, Fe_3O_4@nano-cellulose–OPO_3H (Fe_3O_4@NCs–PA) was synthesized as a new magnetic bio-based nanocatalyst and then it was successfully applied to the synthesis of 2-oxo dihydropyrrole derivatives *via* the four-component reaction of dialkylacetylenedicarboxylate, aldehyde, and amines.

Results and discussion

The sequential step for the preparation of Fe_3O_4@NCs–PA has been shown in Scheme 1. At first, nano-cellulose was prepared from cotton using the previously reported method.[41] Then, magnetic core–shell nanoparticles, Fe_3O_4@nano-cellulose (Fe_3O_4@NCs), were obtained simply through *in situ* co-precipitation of ferric and ferrous ions with ammonium hydroxide in an aqueous solution containing nano-cellulose.[41] At the end, the Fe_3O_4@nano-cellulose served as a magnetic support for the immobilization of $–OPO_3H$ groups by simple grinding with P_2O_5 at room temperature (Scheme 1). The characterization of Fe_3O_4@NCs–PA structure was performed by FT-IR, FESEM, XRD, TGA, VSM, EDX, XRF and BET analyses.

Fig. 1 shows the FT-IR (ATR) spectra of nano-cellulose, Fe_3O_4@NCs and Fe_3O_4@NCs–PA. In the FT-IR spectrum of nano-cellulose (Fig. 1(a)), the signals related to the O–H and C–O stretching vibrations appeared at 3000–3600 cm^{-1} and 1027–1157 cm^{-1}, respectively. In the FT-IR spectrum of Fe_3O_4@NCs (Fig. 1(b)), in addition to the above mentioned bands, a broad band at around 550–660 cm^{-1} shows Fe–O stretching vibrations reflecting the formation of a nano-cellulose shell around the Fe_3O_4 nano-particles. Successful $–OPO_3H$ groups functionalization on Fe_3O_4@NCs was also confirmed by the appearance of new bands at 2650–2700, 1150–1220 and 940–1100 cm^{-1} attributed to the stretching vibrations of PO–H, P=O, P–OH bonds, respectively (Fig. 1(c)).

Fig. 2 represents the result of field emission scanning electron microscopy (FESEM) of Fe_3O_4@NCs–PA to investigate its particle size and surface morphology. This image indicates that Fe_3O_4@NCs–PA nanoparticles have a quasi-spherical shape with an average size about 60 nm.

The comparison between Fe_3O_4, Fe_3O_4@NCs and Fe_3O_4@NCs–PA, XRD patterns in a range of 5–70° was shown in Fig. 3. In Fe_3O_4@NCs XRD pattern, in addition to all peaks of naked Fe_3O_4 ($2\theta = 30°, 35°, 43°, 53°, 57°, 63°, 71°$ and 73°), $2\theta = 23°$ confirmed the existence of cellulose in its structure. The difference between XRD patterns of Fe_3O_4@NCs and Fe_3O_4@NCs–PA shows the additional weak diffraction peaks at

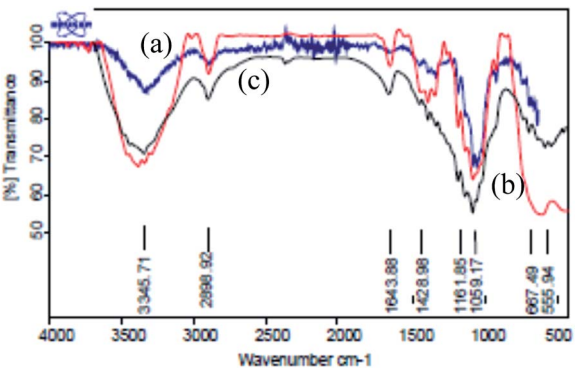

Fig. 1 FT-IR spectra of (a) nano-cellulose, (b) Fe_3O_4@NCs, (c) Fe_3O_4@NCs–PA.

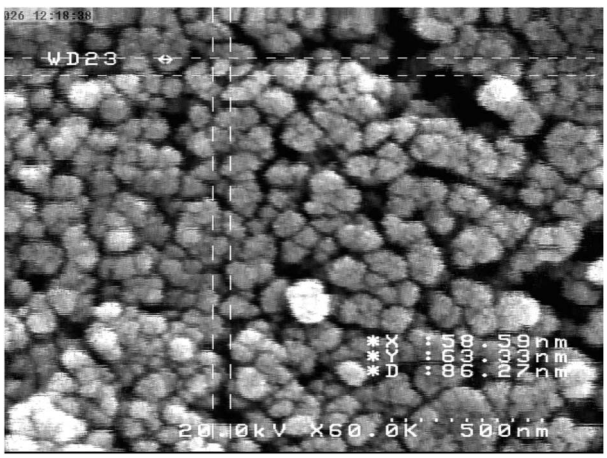

Fig. 2 FESEM image of Fe_3O_4@NCs–PA.

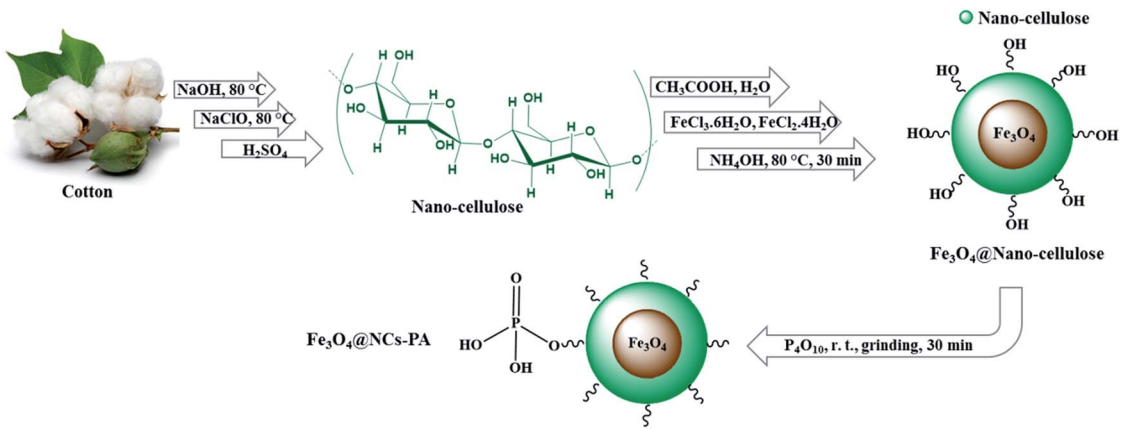

Scheme 1 Graphical representation preparation of Fe_3O_4@nano-cellulose–OPO_3H.

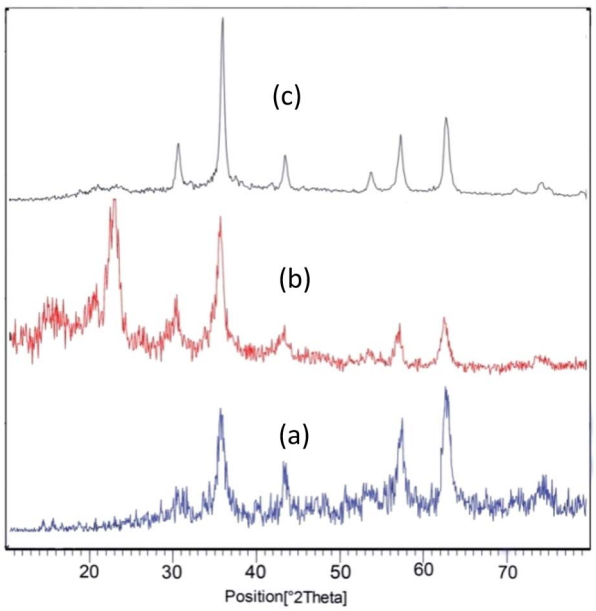

Fig. 3 XRD patterns of the (a) Fe_3O_4 (b) Fe_3O_4@NCs and (c) Fe_3O_4@NCs–PA.

$2\theta = 21°$, 32° and 42° in Fe_3O_4@NCs–PA, which seems to be linked to $-PO_3H$ on the surface of Fe_3O_4@NCs (Fig. 3(c)).

TGA-DTA analysis was performed to estimate thermal stability of the Fe_3O_4@NCs–PA in the temperature range of 32–770 °C (Fig. 4). The first decrease of weight was assigned to the catalyst moisture removal (endothermic effect at 100–200 °C, 4% weight loss) while the second decrease showed the decomposition and burning of cellulose in the nanocomposite (exothermal effect 200–330 °C, 32% weight loss). The char yield of the catalyst in 770 °C is 50.16%.

The magnetic properties of Fe_3O_4, Fe_3O_4@NCs, and Fe_3O_4@NCs–PA were characterized at RT (300 K) by a vibrating sample magnetometer (VSM) and their hysteresis curves are presented in Fig. 5. According to this image, the zero coercivity and remanence of the hysteresis loops of these magnetic nanoparticles confirm superparamagnetic property at room temperature. The amount of specific saturation magnetization (M_s) for Fe_3O_4 nanoparticles was about 47 emu g^{-1}, which decreased to 32 emu g^{-1} after coating the Fe_3O_4 with cellulose and to 12 emu g^{-1} after the immobilization of $-PO_3H$ on the

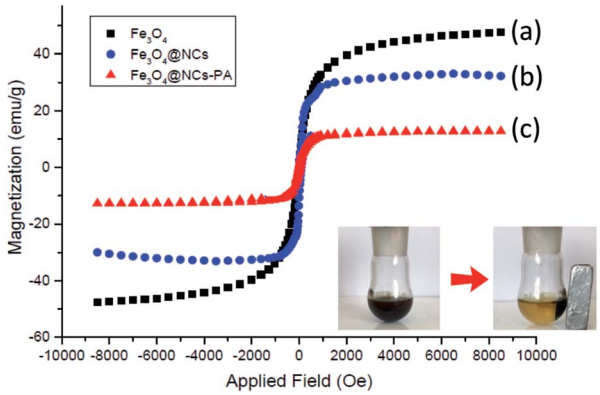

Fig. 5 Magnetization loops of (a) Fe_3O_4, (b) Fe_3O_4@NCs and (c) Fe_3O_4@NCs–PA.

surface of Fe_3O_4@NCs. Despite this significant decrease, the saturated magnetization of these magnetic nanoparticles is sufficient for magnetic separation.

The existence of the expected elements in the structure of the Fe_3O_4@NCs–PA was approved by energy-dispersive X-ray spectroscopy EDS (EDX) analysis (Fig. 6). The EDS results clearly confirm the presence of Fe, O, P, C elements in the catalyst. According to this data, the elemental compositions of Fe_3O_4@NCs–PA were found to be 11.75, 54.42, 3.69 and 30.14% for Fe, O, P and C, respectively. The weight percentages of Fe, O, P and C are 32.75, 43.46, 5.72 and 18.07, respectively.

In addition to EDX analysis, X-ray fluorescence (XRF) analysis of Fe_3O_4@NCs–PA also indicates that the ratio of $Fe_2O_3 : P_2O_5 : CO_2$ is equal to 4.76 : 15.6 : 78.9%. And so, inductively coupled plasma (ICP) analysis of catalyst shows 4.95% P and 21.1% of Fe.

The specific surface area of catalyst was measured by Brunauer–Emmett–Teller (BET) theory. The single point surface area at $P/P_0 = 0.989$ is 2.85 m^2 g^{-1}, while the mean pore diameter is 12.612 nm and the total pore volume is 9.0032 cm^3 g^{-1}. The N_2 adsorption isotherm of catalyst is depicted in Fig. 7. The total acid capacity was found to be in the range of 0.50 mmol g^{-1}, which was determined through the neutralization titration.

The catalytic activity of Fe_3O_4@NCs–PA was investigated for the synthesis of different 2-oxo dihydropyrroles derivatives

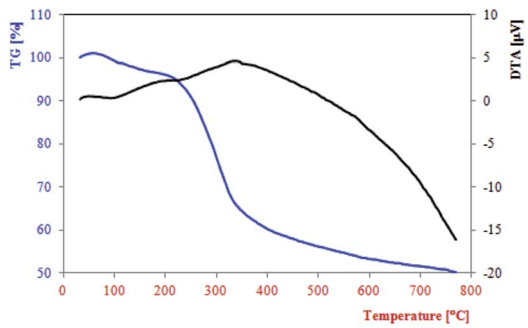

Fig. 4 Thermal gravimetric analysis pattern of Fe_3O_4@NCs–PA.

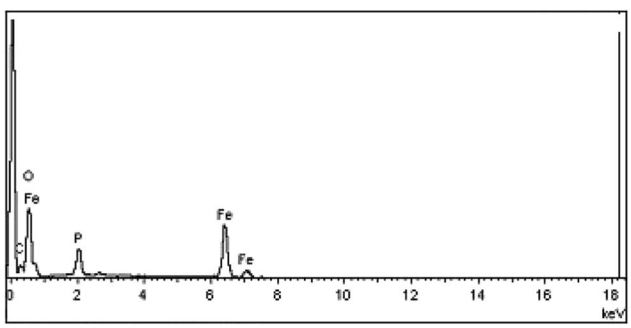

Fig. 6 EDX patterns of Fe_3O_4@NCs–PA.

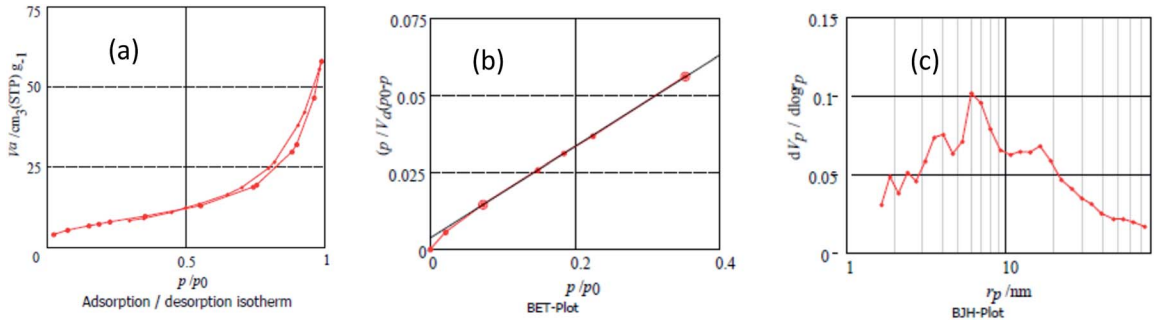

Fig. 7 (a) BET (Brunauer–Emmett–Teller), (b) adsorption/desorption isotherm and (c) BJH (Barrett–Joyner–Halenda) plots of Fe_3O_4@NCs–PA.

Table 1 The reaction of dimethylacetylendicarboxylate, 4-chloroaniline, and formaldehyde in the presence of Fe_3O_4@NCs–PA under various conditions[a]

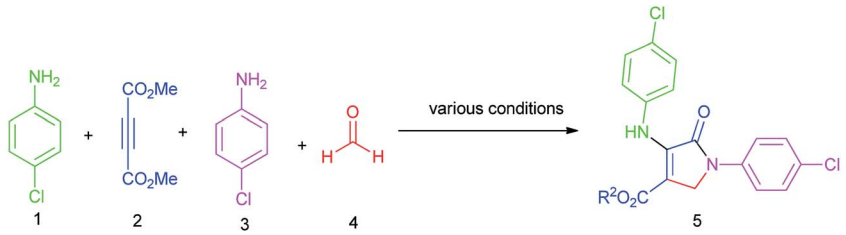

	Conditions					
Entry	Catalyst (g)	Solvent	1 : 2 : 3 : 4 (mmol)	Temperature (°C)	Time (h)	Yield[b] (%)
1	Fe_3O_4@NCs–PA (0.05)	—	1 : 1 : 1 : 1	90	3	35
2	Fe_3O_4@NCs–PA (0.05)	MeOH	1 : 1 : 1 : 1	65	3	54
3	Fe_3O_4@NCs–PA (0.05)	$CHCl_3$	1 : 1 : 1 : 1	60	3	35
4	Fe_3O_4@NCs–PA (0.05)	*n*-Hexane	1 : 1 : 1 : 1	68	3	40
5	Fe_3O_4@NCs–PA (0.05)	H_2O	1 : 1 : 1 : 1	100	3	15
6	Fe_3O_4@NCs–PA (0.05)	EtOH	1 : 1 : 1 : 1	78	3	56
7	Fe_3O_4@NCs–PA (0.05)	EtOH	1 : 1 : 1 : 1	25	3	54
8	Fe_3O_4@NCs–PA (0.05)	EtOH	1 : 1 : 1 : 1.5	78	3	82
9	Fe_3O_4@NCs–PA (0.05)	EtOH	1 : 1 : 1.5 : 1.5	78	3	87
10	Fe_3O_4@NCs–PA (0.05)	EtOH	1 : 1 : 1.5 : 1.5	r.t.	3.5	83
11	Fe_3O_4 MNPs (0.05)	EtOH	1 : 1 : 1.5 : 1.5	r.t.	3.5	38
12	Fe_3O_4@NCs–PA (0.05)	EtOH	1 : 1 : 1.5 : 1.5	r.t.	3.5	35
13	—	EtOH	1 : 1 : 1.5 : 1.5	r.t.	5	5
14	Fe_3O_4@NCs–PA (0.03)	EtOH	1 : 1 : 1.5 : 1.5	r.t.	3.5	78
15	Fe_3O_4@NCs–PA (0.07)	EtOH	1 : 1 : 1.5 : 1.5	r.t.	3.5	88
16	Fe_3O_4@NCs–PA (0.09)	EtOH	1 : 1 : 1.5 : 1.5	r.t.	3.5	88

[a] The molar ratios are 1 (1 mmol), 2 (1 mmol), 3 (1–1.5 mmol) and 4 (1–1.5 mmol). [b] Isolated yield.

via one-pot reaction of amines, aldehydes and dialkylacetylenedicarboxylates in two steps. As a model reaction, the reaction between dimethyl acetylenedicarboxylate, 4-chloroaniline and formaldehyde was investigated under various conditions (Table 1). As can be seen from Table 1, the maximum yield of methyl-1-(4-chlorophenyl)-4-((4-chlorophenyl)amino)-5-oxo-2,5-dihydro-1*H*-pyrrole-3-carboxylate was obtained in the molar ratio of 1 : 1 : 1.5 : 1.5 (1 : 2 : 3 : 4) by using 0.07 g catalyst at room temperature after 3.5 h (Table 1, entry 15). The previously reported protocol was modified by changing the priority of substance addition to reaction vessel. In the first step, in two separated vessels, dimethyl acetylenedicarboxylate with 4-chloroaniline (molar ratio 1 : 1, vessel A) and formaldehyde, 4-chloroaniline (molar ratio 1.5 : 1.5) and 0.07 g of catalyst (vessel B) were charged and mixed at room temperature. In the second step, the resulting mixture in vessel A was added to vessel B and mixed at room temperature for 3.5 h. Using the optimal reaction conditions, the scope and the versatility of this catalytic protocol were explored for the synthesis of various 2-oxo dihydropyrroles (Table 2). The obtained results indicate that the

Table 2 Synthesis of 2-oxo dihydropyrroles derivatives (5a–q) in the presence of Fe_3O_4@NCs–PA at room temperature[a]

Entry	R^1	R^2	R^3	R^4	Product	Time (h)	Yield[b] (%)	Mp (°C) (ref.)
1	4-NO_2–C_6H_4	Et	4-NO_2	H	5a	4	72	207–208 (30)
2	3-NO_2–C_6H_4	Et	3-NO_2	H	5b	4	78	190–191 (30)
3	3-NO_2–C_6H_4	Me	3-NO_2	H	5c	4.5	75	204–206 (30)
4	4-Br–C_6H_4	Et	4-Br	H	5d	3.5	89	164–166 (26)
5	4-Br–C_6H_4	Me	4-Br	H	5e	3.5	90	181–183 (26)
6	4-Cl–C_6H_4	Et	4-Cl	H	5f	4	91	165–167 (27)
7	4-Cl–C_6H_4	Me	4-Cl	H	5g	3.5	88	172–174 (26)
8	4-OMe–C_6H_4	Et	4-OMe	H	5h	3.5	88	153–154 (30)
9	4-OMe–C_6H_4	Me	4-OMe	H	5i	3.5	85	160–162 (25)
10	4-Me–C_6H_4	Et	4-Me	H	5j	3	89	128–129 (25)
11	4-Me–C_6H_4	Me	4-Me	H	5k	3.5	86	176–177 (30)
12	4-Et–C_6H_4	Et	4-Et	H	5l	3	85	102–104 (30)
13	4-Et–C_6H_4	Me	4-Et	H	5m	3	84	124–125 (24)
14	4-Cl–C_6H_4	Me	4-Cl	C_6H_4	5n	3	88	176–177 (26)
15	4-Cl–C_6H_4	Me	4-Cl	4-Me–C_6H_4	5o	4	87	150–151 (30)
16	$PhCH_2$	Me	4-Br	Ph	5p	3.5	90	152–154 (26)
17	$PhCH_2$	Et	H	H	5q	3.5	89	139–141 (30)

[a] The ratio of 1 (mmol) : 2 (mmol) : 3 (mmol) : 4 (mmol) : Fe_3O_4@NCs–PA (g) is 1 : 1 : 1.5 : 1.5 : 0.07. [b] Isolated yields after recrystallization from ethanol.

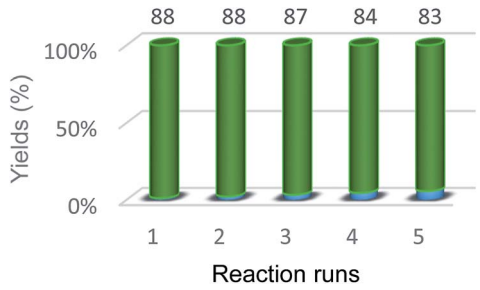

Fig. 8 Catalyst recycling experiments.

reactions can proceed well enough with a relatively wide range of aromatic amines containing electron-donating and electron-withdrawing groups (Table 2, entries 1–15). Additionally, benzylamine acts as a good reactant in this method and the corresponding products are formed in excellent yields (Table 2, entries 16, 17). As shown in Table 2, entries 14 and 15, the reactions are carried out very well with benzaldehyde and 4-methyl benzaldehyde.

The structures of these products were characterized by physical and spectroscopic data such as mp, FT-IR, ^1H NMR, ^{13}C NMR and MS.

In order to investigate the reusability of the catalyst, it was separated by an external magnet following the completion of the reaction and was washed several times with methanol and ethylacetate. The separated catalyst was then dried at room temperature to be used in the subsequent run of the reaction with fresh reactants under similar conditions. It was observed that the recovered magnetite nanoparticles could be used at least five times with marginal decrease in their catalytic activity (Fig. 8). Meanwhile, FT-IR, XRD, VSM spectra and ICP analysis of recovered catalyst were identical with the original catalyst spectra that indicating no considerable leaching of catalyst in reaction medium.

The proposed mechanism for the formation of dihydro-2-oxopyrroles is illustrated in Scheme 2.[28,29] Initially, the amine reacts with formaldehyde in the presence of Fe_3O_4@NCs–PA to form imine A. Also, the Michael reaction between amine and dialkylacetylenedicarboxylate gives enamine B. Activated imine A undergoes a Mannich type reaction with enamine B to generate intermediate C, which converts to more stable tautomeric form D. The intramolecular cyclization in intermediate D forms the desired dihydro-2-oxypyrrole derivatives.

The comparison of data between the efficiency of Fe_3O_4@NCs–PA with other previously reported catalysts for the synthesis of methyl-1-(4-chlorophenyl)-4-((4-chlorophenyl) amino)-5-oxo-2,5-dihydro-1*H*-pyrrole-3-carboxylate (5 g) are shown in Table 3. From environmental friendly and simplicity of protocol viewpoints, the present report is one of the successful methods and is comparable with others. Meanwhile, magnetic property of the applied catalyst in this work cause simpler workup and recovery of catalyst than each other reported procedure.

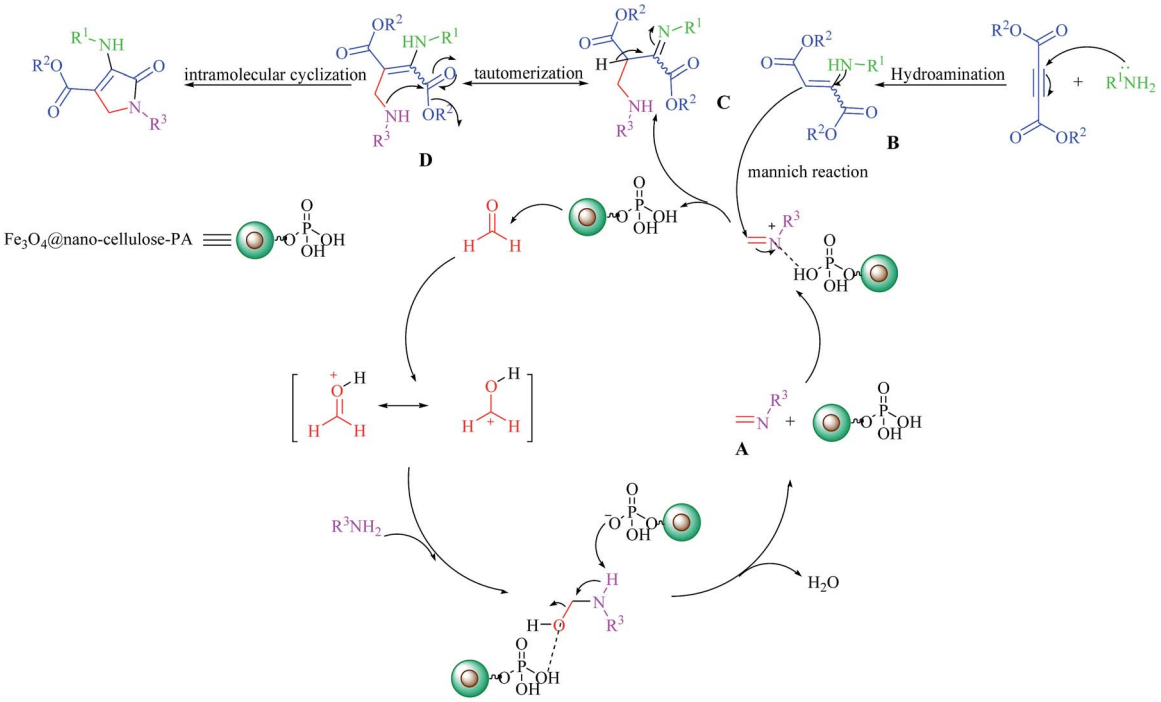

Scheme 2 Proposed mechanism for the synthesis of dihydro-2-oxopyrroles derivatives 5a–q.

Table 3 Catalytic performances of Fe_3O_4@NCs–PA *versus* some other catalysts for synthesis of 5

Entry	Catalyst (mol% or g)	Solvent	Conditions	Molar ratio 1 : 2 : 3 : 4	Time (h)	Yield (%)[ref.]
1	$Al(H_2PO_4)_3$ (0.1 g)	Methanol	r.t.	1 : 1 : 1 : 1.5	6	81 (ref. 44)
2	I_2 (10 mol%)	Methanol	r.t.	1 : 1 : 1.1 : 1.2	1	81 (ref. 24)
3	[*n*-Bu_4N][HSO_4] (10 mol%)	Methanol	r.t.	1 : 1 : 1 : 1.5	4	86 (ref. 27)
4	Cl_3CCO_2H (10 mol%)	Methanol	r.t.	1 : 1 : 1 : 1.5	4	84 (ref. 43)
5	$Cu(OAc)_2 \cdot H_2O$ (15 mol%)	Methanol	r.t.	1 : 1 : 1 : 1.5	6	81 (ref. 26)
6	$InCl_3$ (20 mol%)	Methanol	r.t.	1 : 1 : 1 : 1.5	3	79 (ref. 42)
7	Nano-$TiCl_4/SiO_2$ (0.08 g)	Ethanol	70 °C	1 : 1 : 1 : 3	2	95 (ref. 29)
8	Ph_3CCl (10 mol%)	Ethanol	r.t.	1 : 1 : 1 : 1.5	4	83 (ref. 28)
9	BF_3/nano-sawdust (0.08 g)	Ethanol	Reflux	1 : 1 : 1 : 3	3.5	92 (ref. 30)
10	Fe_3O_4@NCs–PA (0.07 g)	Ethanol	r.t.	1 : 1 : 1.5 : 1.5	3.5	88[present work]

Conclusions

In summary, we have developed the four-component reaction between primary amines, dialkylacetylenedicarboxylates and aldehydes for the synthesis of highly functionalize dihydro-2-oxypyrroles using Fe_3O_4@NCs–PA as a novel bio-based magnetically recyclable catalyst. The present methodology could produce all desired products in good to excellent yields without the need for time-consuming purification procedures. Mild reaction conditions, use of green solvent, high atom-economy and the lack of by-product are among the other advantages of this method.

Experimental

General

All compounds were purchased from Merck, Aldrich and Fluka chemical companies and used without any additional purification. A refrigerated centrifuge (Appendorf Centrifuge 5417R) was used for the preparation of nano-cellulose. FT-IR spectra were run on a Bruker, Equinox 55 spectrometer. A Bruker (DRX-400 Avance) NMR was used to record the ^{1}H-NMR and ^{13}C-NMR spectra. Melting points were determined by a Buchi melting point B-540 B.V.CHI apparatus and were uncorrected. The X-ray diffraction (XRD) pattern was obtained by a Philips Xpert MPD diffractometer equipped with a Cu Kα anode ($k = 1.54$ Å) in the 2θ range from 10 to 80°. Field Emission Scanning Electron Microscopy (FESEM) was obtained on a Mira 3-XMU. XRF analysis was done with Bruker, S4 Explorer instrument. VSM measurements were performed by using a vibrating sample magnetometer (MeghnatisDaghighKavir Co. Kashan Kavir, Iran).

Preparation of Fe_3O_4@NCs–PA

A mixture of synthesized Fe_3O_4@NCs (1 g) and P_2O_5 (2 g) was ground in a mortar at room temperature for 30 minutes to

obtain a glue-like residue. After cooling the reaction mixture, 5 mL of ethanol was added and the obtained catalyst was filtered off, washed with ethanol and dried at room temperature.

General procedure for synthesis of dihydro-2-oxopyrroles

As the first step, a mixture of primary amine (1 mmol), dialkylacetylenedicarboxylate (1 mmol) and absolute ethanol (3 mL) was poured into a 50 mL round-bottom flask (vessel A) and stirred for 15 min at room temperature. Then, the other flask (vessel B) was charged with a mixture of other amine (1.5 mmol), formaldehyde 37% (1.5 mmol), Fe_3O_4@NCs–PA (0.07 g) and absolute ethanol (3 mL). The mixture in vessel B was stirred at room temperature for 30 minutes. In the second step, the contents of vessel A were added to vessel B and the final mixture was stirred at room temperature for appropriate time (monitored by TLC, hexane : EtOAc (80 : 20)). Then the catalyst was separated by an external magnet and the residue mixture was concentrated to obtain crystalline product.

Acknowledgements

The Research Council of Yazd University gratefully acknowledged for the financial support for this work.

References

1 J. H. Clark, *Green Chem.*, 1999, **1**, 1–8.
2 R. A. Sheldon, *Green Chem.*, 2005, **7**, 267.
3 R. A. Sheldon, *Chem. Soc. Rev.*, 2012, **41**, 1437–1451.
4 A. Domling, W. Wang and K. Wang, *Chem. Rev.*, 2012, **112**, 3083–3135.
5 Y. Gu, *Green Chem.*, 2012, **14**, 2091.
6 N. Isambert, M. Sanchez Duque Mdel, J. C. Plaquevent, Y. Genisson, J. Rodriguez and T. Constantieux, *Chem. Soc. Rev.*, 2011, **40**, 1347–1357.
7 P. Slobbe, E. Ruijter and R. V. A. Orru, *MedChemComm*, 2012, **3**, 1189.
8 B. Li, M. P. Lyle, G. Chen, J. Li, K. Hu, L. Tang, M. A. Alaoui-Jamali and J. Webster, *Bioorg. Med. Chem.*, 2007, **15**, 4601–4608.
9 R. Shiraki, A. Sumino, K.-i. Tadano and S. Ogawa, *Tetrahedron Lett.*, 1995, **36**, 5551–5554.
10 T. Kawasuji, M. Fuji, T. Yoshinaga, A. Sato, T. Fujiwara and R. Kiyama, *Bioorg. Med. Chem.*, 2007, **15**, 5487–5492.
11 Y. Mizushina, S. Kobayashi, K. Kuramochi, S. Nagata, F. Sugawara and K. Sakaguchi, *Biochem. Biophys. Res. Commun.*, 2000, **273**, 784–788.
12 L. Zhang, Y. Tan, N. X. Wang, Q. Y. Wu, Z. Xi and G. F. Yang, *Bioorg. Med. Chem.*, 2010, **18**, 7948–7956.
13 A. D. Borthwick, A. J. Crame, P. F. Ertl, A. M. Exall, T. M. Haley, G. J. Hart, A. M. Mason, A. M. K. Pennell, O. M. P. Singh, G. G. Weingarten and J. M. Woolven, *J. Med. Chem.*, 2002, **45**, 1–18.
14 Q. Chen, M. T. Huggins, D. A. Lightner, W. Norona and A. F. McDonagh, *J. Am. Chem. Soc.*, 1999, **121**, 9253–9264.
15 H. He, H. Y. Yang, R. Bigelis, E. H. Solum, M. Greenstein and G. T. Carter, *Tetrahedron Lett.*, 2002, **43**, 1633–1636.
16 H. Uchiro, N. Shionozaki, R. Tanaka, H. Kitano, N. Iwamura and K. Makino, *Tetrahedron Lett.*, 2013, **54**, 506–511.
17 S. Suzuki, T. Hosoe, K. Nozawa, K.-i. Kawai, T. Yaguchi and S.-I. Udagawa, *J. Nat. Prod.*, 2000, **63**, 768–772.
18 D. G. Nagle, V. J. Paul and M. Ann Roberts, *Tetrahedron Lett.*, 1996, **37**, 6263–6266.
19 H. Shiozawa and S. Takahashi, *J. Antibiot.*, 1994, **47**, 851–853.
20 W.-R. Li, S. T. Lin, N.-M. Hsu and M.-S. Chern, *J. Org. Chem.*, 2002, **67**, 4702–4706.
21 R. Shiraki, A. Sumino, K.-i. Tadano and S. Ogawa, *J. Org. Chem.*, 1996, **61**, 2845–2852.
22 R. M. Wiedhopf, E. R. Trumbull and J. R. Cole, *J. Pharm. Sci.*, 1973, **62**, 1206–1207.
23 S. Rana, M. Brown, A. Dutta, A. Bhaumik and C. Mukhopadhyay, *Tetrahedron Lett.*, 2013, **54**, 1371–1379.
24 A. Khan, A. Ghosh and M. M. Khan, *Tetrahedron Lett.*, 2012, **53**, 2622–2626.
25 Q. Zhu, H. Jiang, J. Li, S. Liu, C. Xia and M. Zhang, *J. Comb. Chem.*, 2009, **11**, 685–696.
26 L. Lv, S. Zheng, X. Cai, Z. Chen, Q. Zhu and S. Liu, *ACS Comb. Sci.*, 2013, **15**, 183–192.
27 S. S. Sajadikhah and N. Hazeri, *Res. Chem. Intermed.*, 2013, **40**, 737–748.
28 S. S. Sajadikhah and M. T. Maghsoodlou, *RSC Adv.*, 2014, **4**, 43454–43459.
29 A. Bamoniri, B. B. F. Mirjlili and R. Tarazian, *Monatsh. Chem.*, 2015, **146**, 2107–2115.
30 B. B. F. Mirjalili and R. ZareReshquiyea, *RSC Adv.*, 2015, **5**, 15566–15571.
31 R. Ghorbani-Vaghei, D. Azarifar, S. Daliran and A. R. Oveisi, *RSC Adv.*, 2016, **6**, 29182–29189.
32 J.-N. Zhang, X.-H. Yang, W.-J. Guo, B. Wang and Z.-H. Zhang, *Synlett*, 2017, **6**, 734–737.
33 M. M. Khan, S. Khan, S. Iqbal, Saigal and R. Yousuf, *New J. Chem.*, 2016, **40**, 7504–7512.
34 R. B. Baig and R. S. Varma, *Chem. Commun.*, 2013, **49**, 752–770.
35 V. Polshettiwar, R. Luque, A. Fihri, H. Zhu, M. Bouhrara and J. M. Basset, *Chem. Rev.*, 2011, **111**, 3036–3075.
36 S. Shylesh, V. Schunemann and W. R. Thiel, *Angew. Chem., Int. Ed.*, 2010, **49**, 3428–3459.
37 L. M. Rossi, N. J. S. Costa, F. P. Silva and R. Wojcieszak, *Green Chem.*, 2014, **16**, 2906.
38 A. H. Lu, E. L. Salabas and F. Schuth, *Angew. Chem., Int. Ed.*, 2007, **46**, 1222–1244.
39 A. Maleki and M. Kamalzare, *Catal. Commun.*, 2014, **53**, 67–71.
40 L. Edjlali, R. H. Khanamiri and J. Abolhasani, *Monatsh. Chem.*, 2014, **146**, 1339–1342.
41 S. Azad and B. F. Mirjalili, *RSC Adv.*, 2016, **6**, 96928–96934.
42 S. S. Sajadikhah, M. T. Maghsoodlou and N. Hazeri, *Chin. Chem. Lett.*, 2014, **25**, 58–60.
43 N. Hazeri, M. T. Maghsoodlou, S. Mohamadian-Souri, M. Lashkari and M. Ghashang, *Iran. J. Catal.*, 2015, **5**, 9–14.
44 S. S. Sajadikhah, N. Hazeri, M. T. Maghsoodlou, S. M. Habibi-Khorassani, A. Beigbabaei and A. C. Willis, *J. Iran. Chem. Soc.*, 2013, **10**, 863–871.